ACS APPLIED MATERIALS & INTERFACES

Research Article

www.acsami.org

Organic-free Anatase TiO_2 Paste for Efficient Plastic Dye-Sensitized Solar Cells and Low Temperature Processed Perovskite Solar Cells

Nianqing Fu,[†,‡,§] Chun Huang,[§] Yan Liu,[§] Xing Li,[§] Wei Lu,[§] Limin Zhou,[∥] Feng Peng,[†] Yanchun Liu,*[,‡] and Haitao Huang*[,§]

[†]School of Chemistry and Chemical Engineering, South China University of Technology, Guangzhou 510640, China

[‡]The Key Laboratory of Energy-Efficient Functional Ceramics and Applied Technology of Guangdong Province, Guangzhou Redsun Gas Applications Co., LTD, Guangzhou 510435, China

[§]Department of Applied Physics and Materials Research Center, The Hong Kong Polytechnic University, Hong Kong, China

[∥]Department of Mechanical Engineering, The Hong Kong Polytechnic University, Hong Kong, China

Supporting Information

ABSTRACT: Recently, the synthesis of fine TiO_2 paste with organic-free binder emerged as an indispensable technique for plastic photovoltaics due to the low temperature processing requirement. In this study, pure anatase TiO_2 nanoparticles and organic-free TiO_2-sol were successfully synthesized individually in organic-free solution. By mixing the pure anatase TiO_2 with the newly developed TiO_2-sol binder, mechanically robust and well-interconnected TiO_2 films were prepared via UV-irradiation at low temperature for applications in plastic dye-sensitized solar cells (p-DSSCs). The structural, electrical, and photovoltaic properties of the films as well as the devices were investigated by various techniques. The dye-loading amount of the obtained film is 2.6 times that of the P25 electrodes. As revealed by electrochemical impedance spectroscopy results, the film derived from the as-prepared anatase TiO_2 paste (A-TiO_2) exhibits much smaller charge transport resistance and lower electron recombination rate than the P25 film, while the introduction of TiO_2-sol into the paste can further remarkably decrease the resistance of the produced film (AS-TiO_2). The p-DSSCs employing AS-TiO_2 photoanode yield a high efficiency up to 7.51%, which is 86% higher than the P25 reference cells and also 31% higher than the A-TiO_2 cell. As a proof of concept, the newly developed AS-TiO_2 paste was also applied to low temperature processed perovskite solar cells (PSCs), and a promising high efficiency up to 9.95% was achieved.

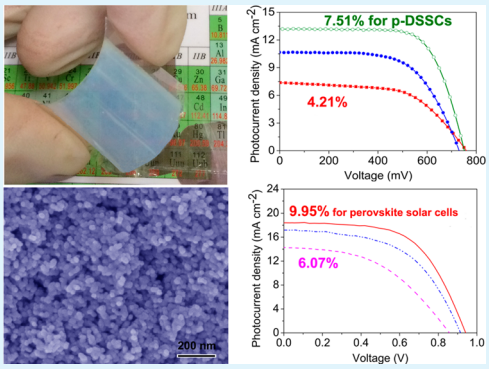

KEYWORDS: *anatase TiO_2, TiO_2-sol, plastic dye-sensitized solar cells, perovskite solar cells, low temperature, organic-free*

1. INTRODUCTION

Owing to the increasingly severe energy-shortage and environmental problems, photovoltaic technology has attracted a great deal of attention. Among various kinds of photovoltaics, dye-sensitized solar cells (DSSCs) and perovskite solar cells (PSCs) have demonstrated their potentials as promising alternatives to silicon based solar cells, because of their low cost, relatively high efficiency, and simple fabrication processes.[1−9] Till now, high efficiency up to 12.3% and 19.3% has been achieved for the transparent conductive oxide (TCO) coated glass based rigid DSSCs and PSCs, respectively.[1,2] Though the flexible DSSCs and PSCs, which are fabricated on flexible substrates, exhibit relatively lower efficiency than the rigid ones, intensive research has been focused on them recently, since they offer some significant advantages over the conventional rigid ones.[5−12] For example, the flexible solar cells are normally lightweight, are easily portable, and can be installed quickly even on nonflat surfaces, expanding the application range significantly.[11] Besides, the plastic devices are usually prepared at low temperature, which not only reduces the production cost significantly but also enables a roll-to-roll mass production.[11]

Fine TiO_2 films for both DSSCs and PSCs are usually deposited on TCO glass by a high temperature sintering procedure employing organic binder contained pastes. The organic binder is used to increase the viscosity of the TiO_2 paste and improve the wettability of the paste to the substrate, enabling the formation of a crack-free film with desirable thickness. A subsequent high temperature sintering at around 450 °C is indispensable for removing the binder and achieving better electric contact between TiO_2 particles.[8,12] However, for flexible substrates, such as ITO coated PEN (polyethylene naphthalate, ITO/PEN) or PET (polyethylene, ITO/PET), the thermal treatment should be restricted to be below 150 °C. Hence the low temperature processing of fine semiconductor photoanodes becomes a big challenge for flexible photovoltaics.

Received: June 25, 2015
Accepted: August 18, 2015
Published: August 18, 2015

DOI: 10.1021/acsami.5b05672
ACS Appl. Mater. Interfaces 2015, 7, 19431−19438

As a key to the low temperature fabrication of crack-free and mechanically robust semiconductor films with good electric connection among particles and tight adhesion to the substrate, the preparation of organic-free TiO_2 paste turns out to be the major challenge faced by high performance plastic photovoltaic devices.[11−15] Recently, several attempts have been tried on the preparation of organic binder-free TiO_2 paste for plastic DSSCs. Miyasaka et al. proposed a "chemical sintering" technique by mixing TiO_2 particles of various sizes to prepare TiO_2 paste,[16,17] where the small particles act as interparticle connection agents to enhance the electrical connection in the deposited film. Ko et al. also reported the addition of TiO_2 nanoglue (containing 5 nm sized TiO_2 particles) into the TiO_2 colloid to form a viscous slurry.[12] The flexible DSSCs derived from this kind of TiO_2 slurry yielded an efficiency of 5.4%.[12] Another method to increase the interconnection among TiO_2 particles was realized by adding a small amount of Ti-monomers into the TiO_2 pastes.[18,19] During the drying process or post-treatment, the Ti-monomers could transfer into TiO_2, forming firm chemical bonding among TiO_2 particles in the deposited film.[18,19] By carefully selecting the solvent and additive, highly viscous and printable TiO_2 pastes were prepared by Park and Cheng, respectively.[20,21] In our previous work, a kind of gel-like TiO_2 paste using a novel (Sb, In)-doped SnO_2 sol as the binder was also developed.[13,14] Owing to the incorporation of the *in situ* formed (Sb, In)-doped SnO_2 nanocrystals with high conductivity, the obtained photoanodes exhibit significant improvement in both mechanical and electrical properties, leading to 49 and 76% increases in power conversion efficiency (PCE) for liquid and quasi-solid state plastic DSSCs, respectively.[13,14] Even though some promising results have been achieved, the PCE of the obtained plastic DSSCs is still relatively low, when compared with the TCO glass based devices. One of the main reasons is the relatively poor electric property of the semiconductor film obtained under low temperature processing. Another reason responsible for the poor cell performance is the commercial P25 powder (with a mixed phase of rutile and anatase at a ratio of 2:8) used. In general, rutile exhibits a much lower capacity to anchor carboxyl (−COOH) group based dyes than anatase,[22−26] which results in a low dye-loading amount for P25 photoanodes and a low PCE of the cell.[22−26] To the best of our knowledge, the highest reported PCE of the plastic DSSC derived from pure P25 is 6.6%.[27] Frank et al. compared the performance of the DSSCs with rutile and anatase based photoanodes and found that the anatase based photoanode showed not only a 35% increase in dye-loading but also faster electron transport.[24] Hence, anatase TiO_2 is preferred for the fabrication of high performance DSSCs. However, until now, most of the attempts on plastic DSSCs are focusing on the development of organic binder-free P25 pastes and the corresponding technique for the deposition of fine semiconductor film at low temperatures,[11−21] without realizing the importance of pure anatase TiO_2 in the organic-free solution.

In our previous work, a novel (Sb, In)-doped SnO_2 sol was developed as an inorganic binder to prepare viscous P25 based paste for plastic DSSCs, and the PCE of the cells was improved from 4.5 to 6.8%.[13] However, the PCE is still lower than 7% due to the use of P25 powder and the doped SnO_2 with a low conduction band (which may act as a recombination center). A higher efficiency is expected by replacing the P25 and doped SnO_2-sol binder with pure anatase TiO_2 nanocrystals and a TiO_2-sol. In this study, pure and organic-free anatase TiO_2 nanoparticles were synthesized by a hydrothermal technique in an acetic acid/water solution, and a novel TiO_2-sol was also prepared and used as a binder. By combining the obtained anatase TiO_2 and TiO_2-sol binder, fine TiO_2 films with excellent performance (in terms of dye-loading capacity, electron transport, and recombination) were deposited on ITO/PEN substrate at low temperature for plastic DSSC application. The low temperature processed TiO_2 paste was also applied to the perovskite solar cells, and a high PCE up to 9.95% was yielded.

2. RESULTS AND DISCUSSION

2.1. Morphological structures of the TiO_2 particles and TiO_2 films. The transmission electron microcopy (TEM) images of the obtained TiO_2 are displayed in Figure 1a. It can

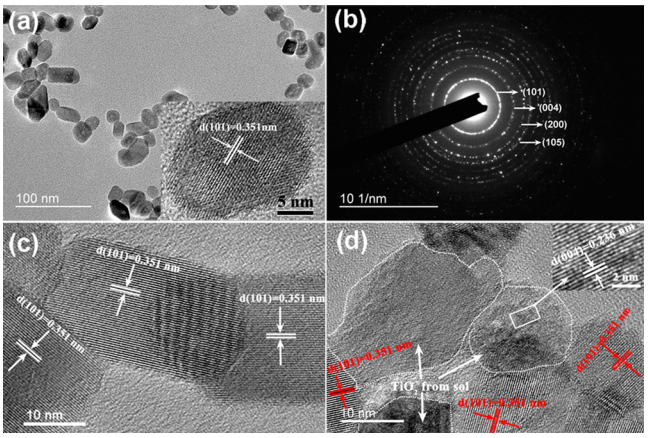

Figure 1. (a) TEM and (b) SAED patterns of the anatase TiO_2 particles. The inset of (a) is the HR-TEM image of an anatase TiO_2 particle. (c) and (d) are the HR-TEM images of samples from the A-TiO_2 and the AS-TiO_2 films, respectively.

be seen that the size of the TiO_2 particles is 15−30 nm with an interlayer spacing of 0.351 nm (inset of Figure 1a), corresponding to the *d*-spacing of (101) planes of anatase TiO_2. The first four diffraction rings in the selected area electron diffraction (SAED) pattern (Figure 1b) can be indexed as the (101), (004), (200), and (105) planes of anatase TiO_2. The diffraction peaks of these planes are centered at 25.32°, 37.82°, 48.06°, and 53.96°, respectively, in the X-ray diffraction (XRD) pattern (Figure 2). Apart from the anatase peaks, no impurity peaks can be identified in the XRD pattern (Figure 2), indicating a pure anatase phase. The calculated crystalline size is 21.4 nm, according to the Scherrer equation. The XRD results are in good agreement with the high resolution-TEM (HR-TEM) and TEM/SAED results. The crystal structure (Figure S1, Supporting Information) determines that anatase can form more surface Ti−OH groups and exhibit higher capacity to couple with carboxyl group based dyes (such as N719) when compared with rutile TiO_2.[22−26] More detailed discussion about the anatase and rutile structures can be found in the Supporting Information. Meanwhile, the Brunauer−Emmett−Teller (BET) surface area of the obtained anatase TiO_2 is 96.3 $m^2\ g^{-1}$, much higher than that of P25 (49.2 $m^2\ g^{-1}$). The larger surface area and the pure anatase phase are beneficial to the anchoring of dye molecules and, hence, the efficiency of the solar cells. The high resolution TEM images of the powders detached from the film prepared by the anatase TiO_2 paste and

DOI: 10.1021/acsami.5b05672
ACS Appl. Mater. Interfaces 2015, 7, 19431−19438

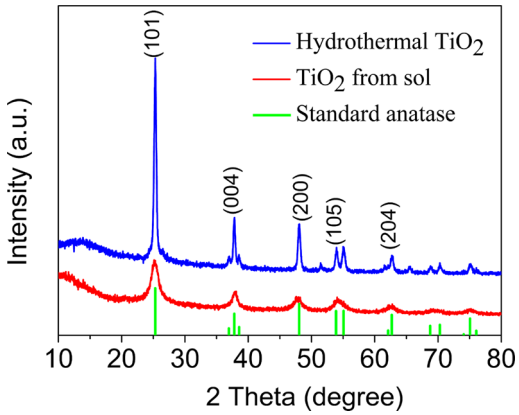

Figure 2. XRD patterns of the hydrothermally prepared anatase TiO_2 (blue) and the TiO_2 (red) from the TiO_2-sol, prepared by UV-irradiation.

TiO_2-sol contained anatase TiO_2 paste (denoted as A-TiO_2 and AS-TiO_2, respectively, hereafter) are displayed in Figures 1 c and 1d, respectively. It reveals that the *in situ* formed TiO_2 nanoparticles from the sol bridge the gap between the anatase TiO_2 particles to form a continuous network which will decrease the electron transport resistance of the AS-TiO_2 film, leading to a fast charge transport and high solar cell performance. The XRD pattern shown in Figure 2 demonstrates that the TiO_2-sol can be crystallized into anatase TiO_2 under UV-irradiation, with an average crystal size around 10.2 nm (calculated from the Scherrer equation). The interlayer spacing of the TiO_2 derived from the sol is 0.236 nm (HR-TEM inset of Figure 1d), corresponding to the *d*-spacing of (004) planes of anatase TiO_2.

The scanning electron microscopy (SEM) images depicting the surface morphologies of the P25, A-TiO_2, and AS-TiO_2 films are displayed in Figure 3. It can be seen that the film produced from A-TiO_2 paste exhibits less cracks than the P25 film, while a smooth and crack-free film can be ultimately achieved in AS-TiO_2. This is because the better solvation of the TiO_2 particles in the hydrothermally produced paste will significantly decrease the surface tension of the paste and leads to a smoother film, when compared with the powder dispersed P25 paste. The addition of the TiO_2-sol, which acts as a binder, decreases the surface tension further.[13,14] High magnification SEM images (Figures 3d-3f) show that the void size in the A-TiO_2 film is much smaller than that in the P25 film, and it is further decreased in the AS-TiO_2 film. In other words, the particle packing densities of the A-TiO_2 and AS-TiO_2 films are higher than those of the P25 film, which results in two benefits. One is the enhanced interconnection among particles and, hence, decreased film resistance, enabling fast charge transport. The other is the increased TiO_2-loading for films of the same thickness, leading to increased total surface area of TiO_2 and hence a higher dye-loading. It should be noted that the large voids left in the P25 film (Figure. 3d) are detrimental to dye absorption, since only a monolayer to N719 molecules is absorbed on the surface of TiO_2, leaving the empty space of large voids wasted. For the 11-μm-thick films, the TiO_2 loadings are 1.23, 2.02, and 2.06 mg·cm^{-2} for P25, A-TiO_2, and AS-TiO_2 films, respectively, and the dye-loadings are 0.98, 2.34, and 2.57 × 10^{-7} mol·cm^{-2}, respectively. The remarkable increase in dye absorption can be easily observed with the naked eye (inset of Figure 3f). Both the enhanced charge transport and improved dye-absorption are desirable for high efficiency DSSCs.

2.2. Electrochemical properties of the electrodes. To investigate the electron transport and transfer processes in DSSCs, electrochemical impedance spectroscopy (EIS) measurements were conducted on various DSSCs, under 1.5 AM illumination in open-circuit conditions. The equivalent circuit for the complete cell can be represented by a transmission line model as depicted in Figure 4a.[28,29] A detailed description of the transmission line model and its characteristic elements can be found from the Supporting Information. The recorded Nyquist plots and Bode phase plots of P25, A-TiO_2, and AS-TiO_2 cells are compared in Figures 4b and 4c. The electrochemical parameters are extracted from the EIS results by fitting the Nyquist plots using the model proposed by Bisquert,[33] and the results are summarized in Table 1. Some key parameters were estimated according to the following expressions:[30,31]

$$\tau_e = \frac{1}{2\pi f_{max}} \quad (1)$$

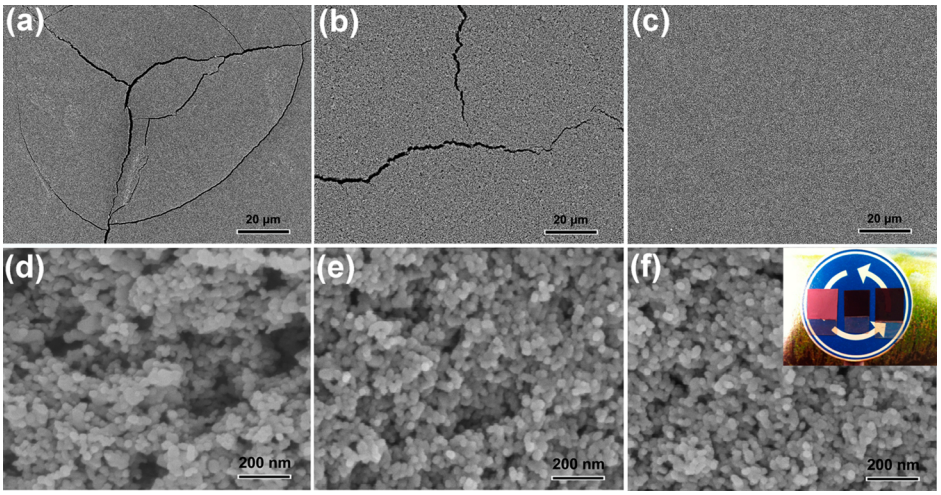

Figure 3. Surface SEM images of the (a) P25, (b) A-TiO_2, and (c) AS-TiO_2 films. (d), (e), and (f) are the corresponding SEM images of a higher magnification. The inset of (f) displays the dye-sensitized electrodes based on P25, A-TiO_2, and AS-TiO_2 (from left to right).

DOI: 10.1021/acsami.5b05672
ACS Appl. Mater. Interfaces 2015, 7, 19431−19438

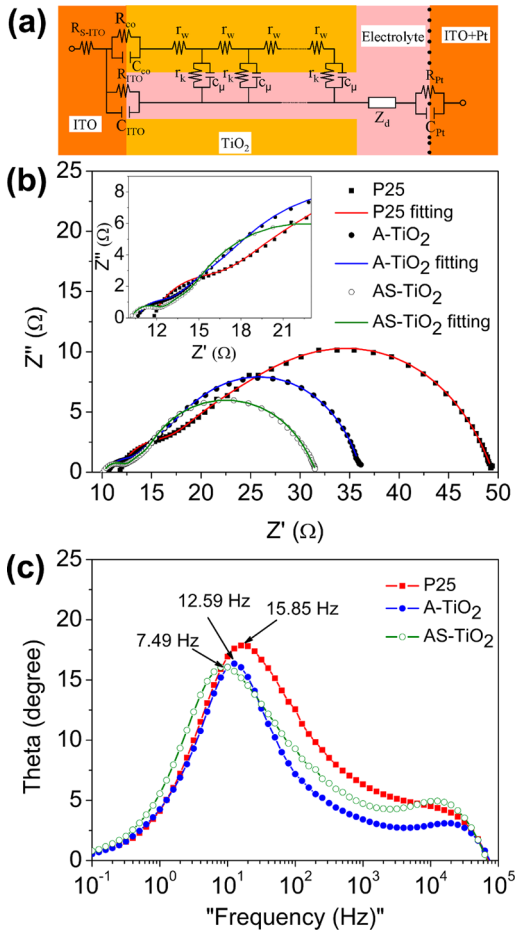

Figure 4. (a) General transmission line model of DSSCs. (b) Nyquist plots and (c) Bode phase plots of DSSCs based on P25, A-TiO_2, and AS-TiO_2 electrodes. The inset of (b) is an enlarged part of the Nyquist plots. The symbols and lines in (b) present the experimental data and fitting results, respectively.

$$k_{\text{eff}} = \frac{1}{\tau_e} \tag{2}$$

$$\eta_{\text{cc}} = 1 - \frac{\tau_{\text{d}}}{\tau_{\text{e}}} = 1 - \frac{R_{\text{w}}}{R_{\text{w}} + R_{\text{k}}} \tag{3}$$

$$R_{\text{s-total}} = R_{\text{s}} + R_{\text{pt}} + R_{\text{co}} + \frac{1}{3}R_{\text{w}} + R_{\text{D}} \tag{4}$$

$$n_{\text{s}} = \frac{k_{\text{B}}T}{q^2 A}\frac{1}{R_{\text{k}}k_{\text{eff}}L} \tag{5}$$

where τ_e is the effective electron lifetime, $f_{\max}$ is the peak frequency corresponding to the second arc in the Nyquist plots, k_{eff} represents the recombination rate, η_{cc} is the charge collection efficiency, and $R_{\text{s-total}}$ is the total series resistance of the device. n_s, k_B, T, q, and A in eq 5 represent the steady state electron density in the conduction band, the Boltzmann constant, the absolute temperature, the charge of a proton, and the electrode area, respectively.[30]

The fitting results reveal that the electron transport resistance, R_w, of A-TiO_2 is 5.87 Ω, which is only about half that of the P25 cell (10.19 Ω). The low R_w value, which is favorable for fast charge transport, is due to the denser packing of the anatase TiO_2 particles in the A-TiO_2 film, as shown in the SEM images (Figure 3). The R_w is further decreased significantly to 3.08 Ω by incorporating the TiO_2-sol into the A-TiO_2 paste to form the AS-TiO_2 film, since the *in situ* formed TiO_2 from the TiO_2-sol can effectively connect the anatase TiO_2 particles to form a continuous electron-pathway in the film. Given that the counter electrodes used in this study are the same (R_{pt} is around 0.55 Ω), the charge transfer resistance at ITO/TiO_2 contact, R_{co}, can be estimated from the first arc of the Nyquist plots. The R_{co} values are 2.85, 1.28, and 0.93 Ω for the P25, A-TiO_2, and AS-TiO_2 cells, respectively. The smaller R_{co} values of A-TiO_2 and AS-TiO_2 are attributed to the strong adhesion and/or chemical bonding between the semiconductor film and the substrate. The decreased R_{co} will facilitate fast electron transfer from the semiconductor film to the conductive substrate and improve the device efficiency. The interfacial charge recombination resistance, R_k, is 27.97, 22.13, and 18.27 Ω for the P25, A-TiO_2, and AS-TiO_2 cells, respectively, according to the Nyquist plots.[26−28,31,32] According to the relation $R_{dc} = {}^1/_3R_w + R_k$, the decreased R_k will lower the *dc* resistance of the device and improve the cell performance, especially the fill factor (*FF*), of the device.[28,30] As $f_{\max}$ of the central arc is 15.85, 12.59, and 7.49 Hz for the P25, A-TiO_2, and AS-TiO_2 cells, respectively, the recombination rate, k_{eff}, is 10, 7.9, and 5 s^{-1}, and the electron lifetime is 10, 12.6, and 20.1 ms for the P25, A-TiO_2, and AS-TiO_2 cells, respectively. One reason for the low k_{eff} is the small resistance (ca. R_w and R_{co}) induced fast charge transport and transfer. Moreover, the value of R_k/R_w is 5.93 for the AS-TiO_2 cell, which is much higher than that of the P25 one (2.74). A higher R_k/R_w is the necessary condition to keep a low charge recombination, a high charge collection efficiency, and a high PCE for a solar cell.[29,30,34] According to eq 5,[30] the steady state electron density, n_s, of our AS-TiO_2 film is 3 times that of the P25 one (12.46×10^{18} vs 4.02×10^{18} cm^{-3}). As listed in Table 2, the dye-loading amount is 2.57×10^{-7} mol·cm^{-2} for the AS-TiO_2 electrode, which is 2.6 times that of the P25 one (0.98×10^{-7} mol·cm^{-2}). The significant increase of the dye-loading amount, arising from the excellent dye-absorbing capacity, the remarkably higher BET surface area of the obtained anatase TiO_2, and the larger TiO_2 nanoparticle packing density of our AS-TiO_2 electrode, is one of the main factors accounting for the higher n_s. More importantly, n_s of the AS-TiO_2 cell is twice that of the A-TiO_2 one (Table 1). Given the similar dye-loadings in the two cells, the higher n_s in the former suggests that the introduction of the TiO_2-sol as a binder plays an important role in reducing photogenerated electron loss by suppressing charge

Table 1. Electron Transport Characteristics, Extracted from the EIS Results of DSSCs with Different Photoanodes[a]

Devices	k_{eff} [s^{-1}]	R_s [Ω]	R_k [Ω]	R_w [Ω]	R_{co} [Ω]	$R_{\text{s-total}}$ [Ω]	n_s [cm^{-3}]	τ_e [ms]	η_{cc} [%]
P25	10	11.66	27.97	10.19	2.85	18.41	4.02×10^{18}	10.0	63.6
A-TiO_2	7.9	10.58	22.13	5.87	1.28	14.32	6.58×10^{18}	12.6	73.5
AS-TiO_2	5	10.29	18.27	3.08	0.93	12.75	12.46×10^{18}	20.1	83.2

[a]The data in the table are the mean values of three similar samples.

DOI: 10.1021/acsami.5b05672
ACS Appl. Mater. Interfaces 2015, 7, 19431−19438

Table 2. TiO_2-Loading and Dye-Loading of Various Electrodes, and Characteristic Photovoltaic Parameters of DSSCs Based on P25, A-TiO_2, and AS-TiO_2 Photoanodes[a]

Electrode	TiO_2-loading [mg cm^{-2}]	Dye-loading [10^{-7} mol cm^{-2}]	J_{sc} [mA cm^{-2}]	V_{oc} [mV]	*FF*	PCE [%]
P25	1.23	0.98	7.82	758	0.708	4.21
TiO_2	2.02	2.34	10.65	735	0.732	5.73
TiO_2+sol	2.06	2.57	13.45	753	0.742	7.51

[a]The data in the table are the mean values of at least three similar samples.

recombination, owing to the fast charge transport resulting from the bridging effect of the *in situ* formed TiO_2 from the TiO_2-sol. The charge collection efficiency, η_{cc}, determined by the electron injection, charge transport and transfer, and charge recombination is one of the most important parameters to evaluate the performance of solar cells.[34] Usually, high η_{cc} will lead to high PCE.[34] The calculated η_{cc} is 63.6% for the P25 cell and is improved to 73.5% for the A-TiO_2 one. Notably, the incorporation of the TiO_2-sol into the paste further improves the η_{cc} to 83.2% for the AS-TiO_2 cell. The remarkable enhancement in η_{cc} of the AS-TiO_2 devices results from the decreased R_w and $R_{co,}$ the increased R_k/R_w ratio, and the improved n_s as well. The improved η_{cc} will lead to a high short circuit current density, J_{sc}, and a high PCE,[30,34] which will be shown later. The $R_{s\text{-}total}$, arising from a sum of different contributions, is another important parameter of DSSCs and can be calculated according to eq 4.[28] As shown in Table 1, the A-TiO_2 exhibits a lower $R_{s\text{-}total}$ value of 14.32 Ω than the P25 cell, while the A-TiO_2 device exhibits the lowest $R_{s\text{-}total}$ (12.75 Ω) among the various devices. The decreased $R_{s\text{-}total}$ results from the small R_w and R_{co}, as demonstrated above, and leads to a good *FF*, favorable for high efficiency solar cells.[28,30,34]

2.3. Photovoltaic performance of the plastic DSSCs. The photovoltaic performances of the A-TiO_2 and AS-TiO_2 based plastic DSSCs were evaluated with the P25 based cell as a reference. The photocurrent density−voltage (*J*−*V*) curves of DSSCs with various photoanodes were measured under AM 1.5 illumination (100 mW cm^{-2}) and are shown in Figure 5. The

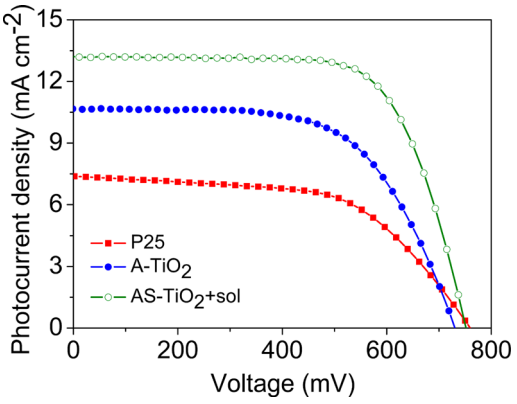

Figure 5. Typical current−voltage curves of plastic DSSCs based on P25, A-TiO_2, and AS-TiO_2 photoanodes, measured under 100 mW cm^{-2}.

corresponding photovoltaic parameters are summarized in Table 2. A PCE of 4.21% was obtained for the P25 cell, with J_{sc} of 7.82 mA·cm^{-2}, an open-circuit voltage (V_{oc}) of 758 mV, and an *FF* of 0.708. The A-TiO_2 cell demonstrated significant enhancements in J_{sc}, V_{oc}, *FF*, and PCE, which are 10.65 mA·cm^{-2}, 735 mV, 0.732, and 5.73%, respectively. Strikingly, an even higher efficiency up to 7.51% was achieved by incorporating the TiO_2-sol into the anatase TiO_2 paste to form the AS-TiO_2 photoanode. The corresponding J_{sc}, V_{oc}, and *FF* of the AS-TiO_2 cell are 13.45 mA·cm^{-2}, 753 mV, and 0.742, respectively. Careful examination of the photovoltaic parameters reveals that the improvements in J_{sc} and *FF* are the main reasons responsible for the remarkable efficiency enhancement. The significant increase in dye-loading amount is one of the main reasons to account for the increased J_{sc}. Additionally, the decreased R_w and R_{co} also lower the photogenerated electron loss by fast charge transport and transfer, resulting in improved J_{sc}.[29,30,34] The low total series resistance ($R_{s\text{-}total}$) of the A-TiO_2 device, as revealed by the EIS measurement, accounts for better *FF*.[28,29,34] Compared with the pristine A-TiO_2, the AS-TiO_2 cell showed a remarkable enhancement in all photovoltaic parameters, that are, 20 mV increase in V_{oc}, 26.3% increase in J_{sc}, and 31.1% increase in PCE. The introduction of the TiO_2-sol as a binder in the anatase A-TiO_2 paste further reduced the electron recombination rate and improved η_{cc}.

It is well-known that the incident photo to current conversion efficiency, IPCE = $\eta_H \times \eta_{inj} \times \eta_{cc}$, is determined by (1) the light harvesting efficiency η_H, (2) the electron injection efficiency η_{inj}, and (3) the electron collection efficiency η_{cc}.[34] As displayed in Figure 6, the IPCE of the A-

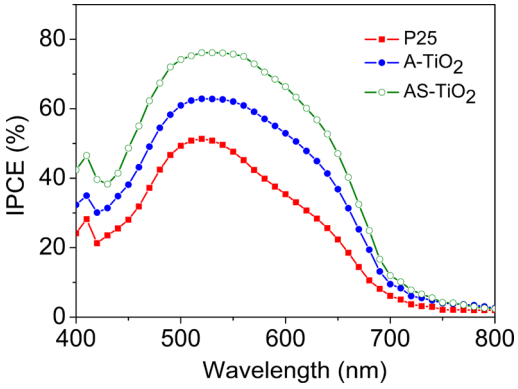

Figure 6. IPCE spectra of the plastic DSSCs with P25, A-TiO_2, and AS-TiO_2 photoanodes.

TiO_2 and AS-TiO_2 cells exhibits a remarkable increase, when compared with their counterpart. The maximum IPCE (at a wavelength ~550 nm) of the A-TiO_2 device is 30% higher than the P25 one (62% vs 47%), and it further increases to 76% (increased by 61.7%) for the AS-TiO_2 device. For the Ru-complex dye used here, the injection of the excited electrons from the dye molecules to the conduction band of TiO_2 is much faster than that of other processes in DSSCs.[28,35−38] A high light harvesting efficiency usually results from a large amount of dye-loading.[24,28,30] In this work, the dye-loading amounts of the A-TiO_2 and AS-TiO_2 electrodes are 2.4 and 2.6 times, respectively, that of the P25 film, while the charge collection efficiencies (estimated from EIS results) increase

DOI: 10.1021/acsami.5b05672
ACS Appl. Mater. Interfaces 2015, 7, 19431−19438

from 63.6% for P25 to 73.5% and 83.2% for A-TiO_2 and AS-TiO_2, respectively. Moreover, it can be found that the IPCEs of the A-TiO_2 and AS-TiO_2 cells increase more significantly in the longer wavelength region (>600 nm) than in the maximum dye absorption region (~550 nm). For example, the IPCE at 680 nm increases by a factor of 1.5 and 2.3 for the A-TiO_2 and AS-TiO_2 cells, respectively, compared with the P25 device. This is due to the fact that, in the longer wavelength regions where the dye absorbs weakly, the photoanode with more dye-loading is more effective to utilize the incident illumination.[24] Therefore, the IPCE enhancement results from the improved light harvesting efficiency and charge collection efficiency. The improved IPCE is in good agreement with the increased J_{sc} observed in Figure 5 and Table 2.

2.4. Photovoltaic performance of the PSCs. Due to the excellent performance of the obtained organic binder-free AS-TiO_2 paste in plastic DSSCs, some preliminary work was carried out to extend its application in low temperature processed perovskite solar cells (PSCs). The primary results (Figure 7 and Table S1) demonstrate that the A-TiO_2 based

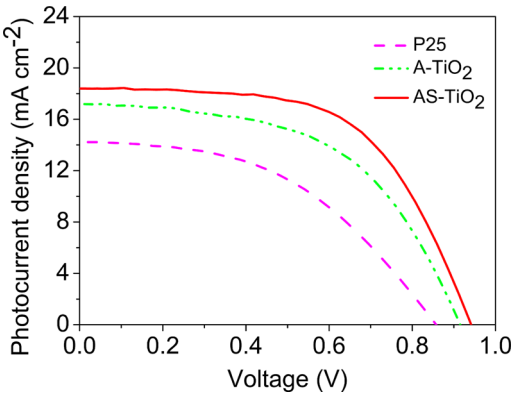

Figure 7. Current–voltage curves of the low temperature processed PSCs based on P25, A-TiO_2, and AS-TiO_2 photoanodes, measured under 100 mW cm^{-2}.

PSC yields a PCE of 8.44%, much higher than the P25 one (6.07%). The J_{sc}, V_{oc}, and *FF* are 17.2 mA·cm^{-2}, 915 mV, and 0.537, respectively, for the A-TiO_2 cell, compared with 14.3 mA·cm^{-2}, 857 mV, and 0.495, respectively, for the P25 one. Similar to the case of DSSC, the AS-TiO_2 based PSC exhibits the best performance among all three types of PSCs, where the J_{sc}, V_{oc}, and *FF* are 18.4 mA·cm^{-2}, 942 mV, and 0.574, respectively, leading to a high PCE, up to 9.95% (64% higher than the P25 one). The enhanced performance of the AS-TiO_2 based PSCs is thought to be resulted from the better crystallinity and smoother morphology of the $CH_3NH_3PbI_{3-x}Cl_x$ layer without pinholes and cracks, as revealed by the SEM image (Figure S3). More detailed discussion can be found from the Supporting Information. The preliminary results presented here demonstrate the potential application of the AS-TiO_2 paste in low temperature processed PSCs.

3. CONCLUSION

In summary, pure anatase TiO_2 nanoparticles and novel TiO_2-sol were successfully synthesized through a hydrothermal process and a sol–gel approach in organic-free solution, respectively. Fine films, namely A-TiO_2 and AS-TiO_2, were deposited on the plastic substrate at low temperature for flexible DSSCs. Owing to the excellent dye-loading capacity and the higher TiO_2-loading, the dye-loading amounts of the A-TiO_2 and AS-TiO_2 films are 2.4 and 2.6 times, respectively, that of the P25 electrode, enabling higher light-harvesting efficiency. The compact packing of anatase particles in film remarkably decreases the electron transport (R_W) resistance of the cells. Acting as a binder, the TiO_2-sol plays an important role in decreasing the R_W and R_k, since it strengthens the connection among the TiO_2 particles and forms a continuous pathway for charge transport in the film. The charge collection efficiency, η_{cc}, of the DSSC was improved from 63.6% (P25) to 73.5% for A-TiO_2 and finally to 83.2% for AS-TiO_2. A PCE of 5.73% was achieved for the A-TiO_2 based plastic DSSC, and it was further increased to 7.51% for the AS-TiO_2 cell due to the addition of the TiO_2-sol, which is 86% higher than the P25 device. The proposed paste was also verified to be applicable to the low temperature processing of plastic perovskite solar cells, where a promising PCE of 9.95% was obtained. Further work toward the higher efficiency of the PSCs is underway. The technique proposed in this work is also promising for the fabrication of plastic photovoltaics which require low temperature processing.

4. EXPERIMENTAL SECTION

4.1. Materials. P25 powders (20–30 nm) was obtained from Degussa (AG, Germany). The Ru dye, cis-di(thiocyanato)-bis(2,2-bipyridyl-4,4-dicarboxylate) ruthenium(II) (N719), was purchased from Solaronix (Switzerland). ITO/PEN substrates (15 Ω sq^{-1}, 82% transparency) were obtained from Peccell. The Titanium(IV) isopropoxide was purchased from Sigma-Aldrich. Other chemicals with analytical purity were purchased from Alfa Aesar and used as received.

4.2. Preparation of TiO_2 particles and TiO_2-sol. The anatase TiO_2 colloid was prepared as follows. 50 mL acetic acid was diluted by 100 mL distilled water (denoted as solution A) and stored in a 4 °C fridge for 2 h. Eighteen mL Titanium(IV) isopropoxide was first mixed with 18 mL iso-propanol and dripped into the solution A under vigorous stirring in an ice–water bath. The mixture was kept stirring overnight. After that, the mixture was heated to 80 °C in an oil bath to evaporate the iso-propanol under vigorous stirring. Two-thirds of the obtained mixture was transferred into a Teflon-lined autoclave with a volume of 200 mL. The hydrothermal treatment was conducted at 240 °C for 12h. After the autoclave was cooled down to room temperature, the resultant white mixture was dispersed by strong ultrasonication to form an uniform TiO_2 colloid (with solid content around 3.5 wt %). TiO_2 colloid with a solid content of 18 wt % for DSSCs was obtained by concentrating the 3.5 wt % colloid via rotary evaporation. The TiO_2-sol was prepared by further evaporating the solvents of the residual one-third mixture in the 80 °C oil bath until a light blue sol with a volume of 22 mL was yielded. The solid content of TiO_2 in the sol was calculated to be 0.074 g·cm^{-2}.

4.3. Preparation of TiO_2 electrodes and assembly of plastic DSSCs. The TiO_2 paste was prepared by blending 2g of the above obtained TiO_2 colloid (18 wt %) with 243 μL TiO_2-sol. P25 paste was also prepared according to our previous work.[13,14] The pastes were coated on the well-cleaned ITO/PEN substrates by the doctor-blade technique. The thickness of the semiconductor films was controlled to be around 11 ± 0.2 μm. After drying at ambient temperature, the electrodes were exposed to UV-irradiation from a 300W mercury lamp for 30 min (the temperature of the electrodes was detected to be around 90 °C during the UV-irradiation) and then sensitized in a 0.5 mM N719 dye/ethanol solution overnight.

The sensitized photoanode with an active area of 0.25 cm^2 was sandwiched with a sputtered Pt/ITO/PEN counter electrode, using a 25 μm Surlyn 1702 film as spacer. The liquid electrolyte composing of 0.5 M LiI, 0.05 M I_2, 0.3 M 1-methyl-3-hexylimidazolium iodide (HMII), 0.3 M *N*-methylbenzimidazole (NMB), and 0.5 M 4-*tert*-

DOI: 10.1021/acsami.5b05672
ACS Appl. Mater. Interfaces 2015, 7, 19431–19438

butylpyridine in 3-methoxypropionitrile was infiltrated between the two electrodes.

4.4. Preparation of PSCs at low temperature. The FTO glass for perovskite solar cells were etched by Zn powder and 2 M HCl solution and cleaned by detergent, acetone, ethanol and DI water successively. An 50 nm compact TiO_2 blocking layer was deposited on the well-cleaned TCO substrate according to the reported work.[2] The TiO_2 paste prepared by blending the 3.5 wt % colloid (5 g) with 118 μL TiO_2-sol was spin-coated on the blocking layer at 2000 rpm for 30 s to form a ~ 400 nm mesoporous layer. The as-coated film was dried at room temperature, exposed to UV-irradiation for 30 min, and finally immersed in plenty of 100 °C DI water for 1 h to remove any absorbed acetic acid on the TiO_2 surface. The CH_3NH_3I was prepared according to the literature.[2] The $PbCl_2$ and CH_3NH_3I with a mole ratio of 1:3 was mixed in the DMF, the concentration of the solution was 0.8 mol/L (with respect to $PbCl_2$). This solution was spin-coated onto the TiO_2 electrodes at 3000 rpm for 30 s. The as prepared film was placed on a hot plate at 105 °C for 2 h to complete the crystallization of the $CH_3NH_3PbI_{3-x}Cl_x$. For the hole transport material (HTM) layer, 30 μL solution composing of 61 mM spiro-OMeTAD, 55 mM *tert*-butylpyridine (TBP) and 26 mM lithium bis-(trifluoromethylsulfonyl)imide salt in chlorobenzene was spin-coated on the perovskite layer at 2000 rpm for 40 s. Finally, 15 nm MoO_3 and 80 nm silver layers were thermal evaporated in sequence onto the masked electrode to complete the fabrication of the PSCs.

4.5. Measurements and characterizations. The microstructures of the TiO_2 particles/films were studied by transmission electron microscope (TEM, JEOL JEM-2100F) and field-emission scanning electron microscope (FESEM, FEI Sirion 200). The anchored dye was desorbed in 0.1 M NaOH aqueous solution and the absorbance was measured by UV−vis spectrophotometer (Model UV-2550, Shimadzu, Japan) to determine the dye-loading amount. X-ray diffraction patterns (XRD, Rigaku 9KW SmartLab, Japan) were recorded for crystal phase identification. *I*−*V* characteristics were recorded on a Keithley 2420 source meter under AM 1.5 G illumination (100 mW cm^{-2}) supplied by a 300 W solar simulator (Model 69911, Newport-Oriel Instruments, USA) which was calibrated using a silicon reference cell (NIST) equipped with a power meter. The IPCE measurements were conducted on a Newport 2931-C power meter. The light source was provided by a Newport 66902 solar simulator, and the wavelength of light was tuned with a Newport 74125 monochromator. The electrochemical impedance spectra (EIS) were collected under AM 1.5 G illumination, using a CHI instrument (CHI 660C, CH Instruments, USA) at the open circuit voltage with an ac perturbation signal of an amplitude 10 mV and a frequency within 10^{-2} to 10^5 Hz.

■ ASSOCIATED CONTENT

Supporting Information

The Supporting Information is available free of charge on the ACS Publications website at DOI: 10.1021/acsami.5b05672.

Schematic structure and detailed description of the anatase and rutile TiO_2, description of the transmission line model, more photovoltaic results, and SEM images of the perovskite solar cells. (PDF)

■ AUTHOR INFORMATION

Corresponding Authors

*E-mail address: aphhuang@polyu.edu.hk (H. Huang). Tel: +852-2766-5694. Fax: +852-2333-7629.

*E-mail address: lyc21@163.com (Y. Liu). Tel: 020-36372332. Fax: 020-22855228.

Notes

The authors declare no competing financial interest.

■ ACKNOWLEDGMENTS

This work was supported by the China Postdoctoral Science Foundation (2014M562167) and the Hong Kong Polytechnic University (Grant Nos. G-UC69 and G-SB27).

■ REFERENCES

(1) Yella, A.; Lee, H. W.; Tsao, H. N.; Yi, C. Y.; Chandiran, A. K.; Nazeeruddin, M. K.; Diau, E. W. G.; Yeh, C. Y.; Zakeeruddin, S. M.; Grätzel, M. Porphyrin-Sensitized Solar Cells with Cobalt (II/III)−Based Redox Electrolyte Exceed 12% Efficiency. *Science* **2011**, *334*, 629−634.

(2) Zhou, H. P.; Chen, Q.; Li, G.; Luo, S.; Song, T. B.; Duan, H. S.; Hong, Z. R.; You, J. B.; Liu, Y. S.; Yang, Y. Interface Engineering of Highly Efficient Perovskite Solar Cells. *Science* **2014**, *345*, 542−546.

(3) Im, J. H.; Jang, I. H.; Pellet, N.; Grätzel, M.; Park, N. G. Growth of $CH_3NH_3PbI_3$ Cuboids with Controlled Size for High-Efficiency Perovskite Solar Cells. *Nat. Nanotechnol.* **2014**, *9*, 927−932.

(4) Chung, I.; Lee, B.; He, J. q.; Chang, R. P. H.; Kanatzidis, M. G. All-Solid-State Dye-Sensitized Solar Cells with High Efficiency. *Nature* **2012**, *485*, 486−490.

(5) Dürr, M.; Schmid, A.; Obermaier, M.; Rosselli, S.; Yasuda, A.; Nelles, G. Low-Temperature Ffabrication of Dye-Sensitized Solar Cells by Transfer of Composite Porous Layers. *Nat. Mater.* **2005**, *4*, 607−611.

(6) Wu, J. H.; Xiao, Y. M.; Tang, Q. W.; Yue, G. T.; Lin, J. M.; Huang, M. H.; Huang, Y. F.; Fan, L. Q.; Lan, Z.; Yin, S.; Sato, T. A Large-Area Light-Weight Dye-Sensitized Solar Cell based on All Titanium Substrates with an Efficiency of 6.69% Outdoors. *Adv. Mater.* **2012**, *24*, 1884−1888.

(7) Fu, N. Q.; Fang, Y. Y.; Duan, Y. D.; Zhou, X. W.; Xiao, X. R.; Lin, Y. High-Performance Plastic Platinized Counter Electrode *via* Photoplatinization Technique for Flexible Dye-Sensitized Solar Cells. *ACS Nano* **2012**, *6* (11), 9596−9605.

(8) Zardetto, V.; Giacomo, Francesco. D.; Garcia-Alonso, D.; Keuning, W.; Creatore, M.; Mazzuca, C.; Reale, A.; Carlo, A. D.; Brown, T. M. Fully Plastic Dye Solar Cell Devices by Low-Temperature UV-Irradiation of both the Mesoporous TiO_2 Photo- and Platinized Counter-Electrodes. *Adv. Energy Mater.* **2013**, *3*, 1292−1298.

(9) Roldán-Carmona, C.; Malinkiewicz, O.; Soriano, A.; Espallargas, G. M.; Garcia, A.; Reinecke, P.; Kroyer, T.; Dar, M. I.; Nazeeruddin, M. K.; Bolink, H. J. Flexible High Efficiency Perovskite Solar Cells. *Energy Environ. Sci.* **2014**, *7*, 994−997.

(10) Docampo, P.; Ball, J. M.; Darwich, M.; Eperon, G. E.; Snaith, H. J. Efficient Organometal Trihalide Perovskite Planar-Heterojunction Solar Cells on Flexible Polymer Substrates. *Nat. Commun.* **2013**, *4* (2761), 1−6.

(11) Weerasinghe, H. C.; Huang, F. Z.; Cheng, Y. B. Fabrication of Flexible Dye Sensitized Solar Cells on Plastic Substrates. *Nano Energy* **2013**, *2*, 174−189.

(12) Li, Y.; Yoo, K.; Lee, D. K.; Kim, J. Y.; Kim, H.; Kim, B. S.; Ko, M. J. Photovoltaic Properties of High Efficiency Plastic Dye-Sensitized Solar Cells Employing Interparticle Binding Agent "Nanoglue. *Nanoscale* **2013**, *5*, 4711−4719.

(13) Fu, N. Q.; Duan, Y. D.; Fang, Y. Y.; Zhou, X. W.; Xiao, X. R.; Lin, Y. Plastic Dye-Sensitized Solar Cells with Enhanced Performance Prepared from a Printable TiO_2 Paste. *Electrochem. Commun.* **2013**, *34*, 254−257.

(14) Fu, N. Q.; Duan, Y. D.; Fang, Y. Y.; Zhou, X. W.; Liu, Y. C.; Peng, F.; Lin, Y.; Huang, H. T. Facile Fabrication of Highly Porous Photoanode at Low Temperature for All-Plastic Dye-Sensitized Solar Cells with Quasi-Solid State Electrolyte. *J. Power Sources* **2014**, *271*, 8−15.

(15) Yin, X.; Xue, Z. S.; Wang, L.; Cheng, Y. M.; Liu, B. High-Performance Plastic Dye-sensitized Solar Cells Based on Low-Cost Commercial P25 TiO_2 and Organic Dye. *ACS Appl. Mater. Interfaces* **2012**, *4*, 1709−1715.

DOI: 10.1021/acsami.5b05672
ACS Appl. Mater. Interfaces 2015, 7, 19431−19438

(16) Miyasaka, T.; Ikegami, M.; Kijitori, Y. Photovoltaic Performance of Plastic Dye-Sensitized Electrodes Prepared by Low-Temperature Binder-Free Coating of Mesoscopic Titania. *J. Electrochem. Soc.* **2007**, *154* (5), A455−A461.
(17) Li, X.; Lin, H.; Li, J. B.; Li, X. X.; Cui, B.; Zhang, L. Z. A Numerical Simulation and Impedance Study of the Electron Transport and Recombination in Binder-Free TiO_2 Film for Flexible Dye-Sensitized Solar Cells. *J. Phys. Chem. C* **2008**, *112*, 13744−13753.
(18) Zhang, D. S.; Yoshida, T.; Minoura, H. Low-Temperature Fabrication of Efficient Porous Titania Photoelectrodes by Hydrothermal Crystallization at the Solid/Gas Interface. *Adv. Mater.* **2003**, *15*, 814−817.
(19) Zhang, D. S.; Yoshida, T.; Oekermann, T.; Furuta, K.; Minoura, H. Room Temperature Synthesis of Porous Nanoparticulate TiO_2 Films for Flexible Dye-Sensitized Solar Cells. *Adv. Funct. Mater.* **2006**, *16*, 1228−1234.
(20) Park, N. G.; Kim, K. M.; Kang, M. G.; Ryu, K. S.; Chang, S. H.; Shin, Y. J. Chemical Sintering of Nanoparticles: A Methodology for Low-Temperature Fabrication of Dye-Sensitized TiO_2 Films. *Adv. Mater.* **2005**, *17*, 2349−2353.
(21) Weerasinghe, H. C.; Franks, G. V.; Plessis, J. D.; Simona, G. P.; Cheng, Y. B. Anomalous Rheological Behavior in Chemically Modified TiO_2 Colloidal Paste Prepared for Flexible Dye-Sensitized Solar Cells. *J. Mater. Chem.* **2010**, *20*, 9954−9961.
(22) Labat, F.; Baranek, P.; Domain, C.; Minot, C.; Adamo, C. Density Functional Theory Analysis of the Structural and Electronic Properties of TiO_2 Rutile and Anatase Polytypes: Performances of Different Exchange-Correlation Functionals. *J. Chem. Phys.* **2007**, *126*, 154703−1−12.
(23) Labat, F.; Baranek, P.; Adamo, C. Structural and Electronic Properties of Selected Rutile and Anatase TiO_2 Surfaces: An ab Initio Investigation. *J. Chem. Theory Comput.* **2008**, *4*, 341−352.
(24) Park, N. G.; Lagemaat, J.; Frank, A. J. Comparison of Dye-Sensitized Rutile-and Anatase-Based TiO_2-solar Cells. *J. Phys. Chem. B* **2000**, *104*, 8989−8994.
(25) De Angelis, F.; Fantacci, S.; Selloni, A.; Grätzel, M.; Nazeeruddin, M. K. Influence of the Sensitizer Adsorption Mode on the Open-Circuit Potential of Dye-Sensitized Solar Cells. *Nano Lett.* **2007**, 7 (10), 3189−3195.
(26) Lee, K. E.; Gomez, M. A.; Elouatik, S.; Demopoulos, G. P. Further Understanding of the Adsorption Mechanism of N719 Sensitizer on Anatase TiO_2 Films for DSSC Applications Using Vibrational Spectroscopy and Confocal Raman Imaging. *Langmuir* **2010**, *26* (12), 9575−9583.
(27) Brown, T. M.; Rossi, F. D.; Giacomo, F. D.; Mincuzzi, G.; Zardetto, V.; Realea, A.; Carlo, A. D. Progress in Flexible Dye Solar Cell Materials, Processes and Devices. *J. Mater. Chem. A* **2014**, *2*, 10788−10817.
(28) Wang, Q.; Ito, S.; Grätzel, M.; Fabregat-Santiago, F.; Mora-Seró, I.; Bisquert, J.; Bessho, T.; Imai, H. Characteristics of High Efficiency Dye-Sensitized Solar Cells. *J. Phys. Chem. B* **2006**, *110*, 25210−25221.
(29) Fabregat-Santiago, F.; Bisquert, J.; Palomares, E.; Otero, L.; Kuang, D. B.; Zakeeruddin, S. M.; Grätzel, M. Correlation between Photovoltaic Performance and Impedance Spectroscopy of Dye-Sensitized Solar Cells Based on Ionic Liquids. *J. Phys. Chem. C* **2007**, *111*, 6550−6560.
(30) Adachi, M.; Sakamoto, M.; Jiu, J. T.; Ogata, Y.; Isoda, S. Determination of Parameters of Electron Transport in Dye-Sensitized Solar Cells Using Electrochemical Impedance Spectroscopy. *J. Phys. Chem. B* **2006**, *110*, 13872−13880.
(31) Chen, H. W.; Liao, Y. T.; Chen, J. G.; Wu, K. C. W.; Ho, K. C. Fabrication and Characterization of Plastic-Based Flexible Dye-Sensitized Solar Cells Consisting of Crystalline Mesoporous Titania Nanoparticles as Photoanodes. *J. Mater. Chem.* **2011**, *21*, 17511−17518.
(32) Lee, C. H.; Chiu, W. H.; Lee, K. M.; Hsieh, W. F.; Wu, J. M. Improved Performance of Flexible Dye-Sensitized Solar Cells by Introducing an Interfacial Layer on Ti Substrates. *J. Mater. Chem.* **2011**, *21*, 5114−5119.
(33) Bisquert, J. Influence of the Boundaries in the Impedance of Porous Film Electrodes. *Phys. Chem. Chem. Phys.* **2000**, *2*, 4185−4192.
(34) Fisher, A. C.; Peter, L. M.; Ponomarev, E. A.; Walker, A. B.; Wijayantha, K. G. U. Intensity Dependence of the Back Reaction and Transport of Electrons in Dye-Sensitized Nanocrystalline TiO_2-solar Cells. *J. Phys. Chem. B* **2000**, *104*, 949−958.
(35) Persson, P.; Lundqvist, M. J. Calculated Structural and Electronic Interactions of the Ruthenium Dye N3 with a Titanium Dioxide Nanocrystal. *J. Phys. Chem. B* **2005**, *109*, 11918−11924.
(36) De Angelis, F.; Fantacci, S.; Selloni, A.; Nazeeruddin, M. K.; Grätzel, M. Time-Dependent Density Functional Theory Investigations on the Excited States of Ru(II)-Dye-Sensitized TiO_2 Nanoparticles: The Role of Sensitizer Protonation. *J. Am. Chem. Soc.* **2007**, *129*, 14156−14157.
(37) Hamann, T. W.; Jensen, R. A.; Martinson, A. B. F.; Ryswyk, H. V.; Hupp, J. T. Advancing Beyond Current Generation Dye-Sensitized Solar Cells. *Energy Environ. Sci.* **2008**, *1*, 66−78.
(38) Asbury, J. B.; Anderson, N. A.; Hao, E.; Ai, X.; Lian, T. Parameters Affecting Electron Injection Dynamics from Ruthenium Dyes to Titanium Dioxide Nanocrystalline Thin Film. *J. Phys. Chem. B* **2003**, *107*, 7376−7386.

DOI: 10.1021/acsami.5b05672
ACS Appl. Mater. Interfaces 2015, 7, 19431−19438